Journal of Nuclear Materials 406 (2010) 360–364

Contents lists available at ScienceDirect

Journal of Nuclear Materials

journal homepage: www.elsevier.com/locate/jnucmat

Dissociation of Cr-rich $M_{23}C_6$ carbide in Alloy 617 by severe plastic deformation

Tae Sun Jo, Jeong Hun Lim, Young Do Kim *

Department of Materials Science and Engineering, Hanyang University, Seoul 133-791, Republic of Korea

ARTICLE INFO

Article history:
Received 11 June 2010
Accepted 17 September 2010

ABSTRACT

In this study, the dissociation of Cr-rich $M_{23}C_6$ carbides in Alloy 617 was investigated using 50% cold rolling. The major carbides in Alloy 617 consisted primarily of $M_{23}C_6$ carbide and a small amount of M_6C carbide. The lattice parameters of the carbides were determined as 1.070 nm ($M_{23}C_6$) and 1.121 nm (M_6C). The area fraction of the total carbides in Alloy 617 decreased from 3.50% to 1.66% after 50% cold rolling. The $M_{23}C_6$ carbide was dissociated by the carbon traps in dislocations generated during the severe plastic deformation. Alternatively, the area fraction of M_6C carbide increased from 0.06% to 0.37% during the dissociation of $M_{23}C_6$ carbide. The area fraction of M_6C carbide increased due to the formation of M_6C carbide as a result of the relative changes in chemical composition, such as Cr and Mo, during the dissociation of $M_{23}C_6$ carbide.

1. Introduction

High temperature gas-cooled reactors (HTGRs) are high-efficiency systems designed for the economical productions of hydrogen and electricity. Alloy 617 is a possible candidate for the tube material of intermediate heat exchangers (IHXs) and hot gas ducts (HGDs) in HTGRs [1–3]. Alloy 617 is a solid-solution strengthened alloy that shows excellent strength, creep-rupture strength and oxidation resistance at high temperatures [4–6]. The mechanical properties, such as creep resistance, can be improved by the distribution of carbides at grain boundaries and inside the grain [3]. The major carbide in Alloy 617 is $M_{23}C_6$ carbide, along with a small amount M_6C [6]. The major metal elements in $M_{23}C_6$ and M_6C carbide are mainly chromium (Cr) and molybdenum (Mo), respectively. The Mo-rich M_6C carbide is more stable than the Cr-rich $M_{23}C_6$ carbide at a high temperature [6–8]. It has been reported that M_6C carbide is formed by the incorporation of Mo into $M_{23}C_6$ carbide during high temperature aging [9–12]. The coarsened carbides were locally distributed at grain boundaries and inside the grain of Alloy 617. The uniform distribution of fine carbides is required for improved mechanical properties.

The modified-microstructure of Alloy 617 with uniformly distributed and fine carbides could be obtained via dissociation and re-precipitation of carbides. According to several authors [13–16], cementite in pearlitic steel is dissociated due to the presence of carbon traps in dislocations generated during severe plastic deformation. As a result, the carbide of Alloy 617 could be dissociated during severe plastic deformation. However, such dissociation of carbides in Alloy 617 has not yet been investigated.

In this study, the dissociation of carbides in Alloy 617 was demonstrated using cold rolling. The dissociation of carbides by severe plastic deformation was investigated through the associated changes in the internal microstrain in the matrix, the area fraction of the carbide, the carbide precipitate and the chemical composition of the carbide.

2. Experimental procedure

The chemical composition of as-received Alloy 617 is given in Table 1. The As-received Alloy 617 was machined to $50 \times 30 \times 10\ mm^3$ for cold rolling. The thickness of the as-received Alloy 617 was reduced up to 50% by cold rolling at room temperature. The as-received Alloy 617 (AR) and 50% cold-rolled Alloy 617 (CR) were heated to 1050 °C at a heating rate of 10 °C/min without a holding time and then were quenched in water. The samples for microstructural observation were prepared via chemical etching with HCl (100 ml), C_2H_5OH (100 ml) and $CuCl_2$ (5 g). The carbides of each sample were observed using back-scattered electron microscopy (BSEM) equipped with energy dispersion spectroscopy (EDS). The internal microstrain in the matrix after 50% cold rolling was calculated according to the peak broadening of the X-ray diffraction (XRD) patterns. Phase analysis of the carbides was investigated using transmission electron microscopy (TEM). The area fractions of carbides in the matrix were calculated using image analysis, which was performed using 50 images (1000×).

* Corresponding author. Address: 17 Haengdang-dong, Seongdong-ku, Seoul 133-791, Republic of Korea. Tel.: +82 2 2220 0408; fax: +82 2 2220 4230.
E-mail address: ydkim1@hanyang.ac.kr (Y.D. Kim).

0022-3115/$ - see front matter © 2010 Elsevier B.V. All rights reserved.
doi:10.1016/j.jnucmat.2010.09.027

Table 1
Chemical composition of Alloy 617 (wt.%).

	C	Ni	Fe	Si	Mn	Co	Cr	Ti	P	S	Mo	Al	B	Cu
Max.	0.08	53.16	1.49	0.06	0.11	11.58	22.16	0.35	0.003	0.001	9.8	1.12	0.002	0.08

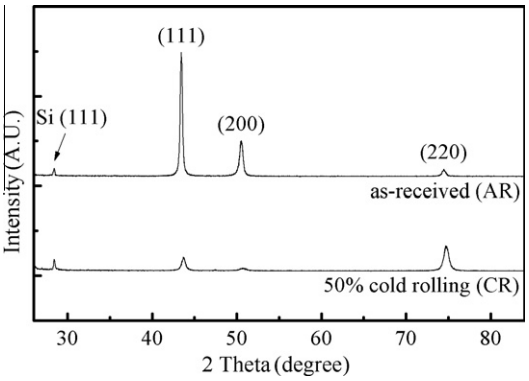

Fig. 1. XRD patterns of the as-received and 50% cold-rolled Alloy 617.

3. Results and discussion

Fig. 1 shows the X-ray diffraction patterns of AR and CR. During cold rolling, shear stress in the specimen was induced by friction between the roll and specimen surface. As shown in the XRD patterns, the texture oriented from the (1 1 1) plane to the (2 2 0) plane was generated by shear stress in the CR. Additionally, internal microstrain can be accumulated in the matrix due to severe plastic deformation and is calculated according to the relationship between peak broadening and non-uniformity of the strain [17]. The internal microstrain is defined as follows:

$$b = \Delta 2\theta = -2\frac{\Delta d}{d}\tan\theta, \tag{1}$$

where b is extra broadening, over and above the instrumental breadth of the line, due to a fractional variation in Bragg plane spacing $\Delta d/d$. This equation allows the variation in the strain, $\Delta d/d$, to be calculated based on the observed broadening. The internal microstrain in CR was calculated as 0.19% using Eq. (1).

The BSE images of AR and CR are presented in Fig. 2. The carbides in AR were locally distributed and globularly shaped with an approximate average size of 4 μm. The major carbides in AR consisted primarily of Cr-rich $M_{23}C_6$ carbide and a small amount of Mo-rich M_6C carbide. Other precipitates, such as MC and Ti(C, N), were rarely observed in Alloy 617. It has been reported that the $M_{23}C_6$ and M_6C carbides are typically composed of Cr_{23-x}(Ni, Co, Mo)$_x$C$_6$ and Mo$_{6-x}$(Cr, Ni, Co)$_x$C, respectively [8]. The dark-colored carbides in AR, which were distributed at grain boundaries and inside the grain, were confirmed as Cr-rich $M_{23}C_6$ carbides containing 22.3 at.% C, 60.4 at.% Cr, 1.8 at.% Co, 5.7 at.% Ni and 9.8 at.% Mo by EDS analysis. Fig. 2b presents the microstructural changes in CR after 50% cold rolling. The grains in CR were elongated in the rolling direction, and the average aspect ratio of the elongated grains increased from 1.7 (AR) to 6 (CR). Moreover, the carbides in CR were fractured during the plastic deformation due to the applied stress and were distributed along the elongated grain boundaries. The carbides in CR resulting from severe plastic deformation were composed of bright and dark carbides. The elementary compositions of bright carbides are thought to have higher atomic numbers compared to those of dark carbides. The bright carbides were confirmed as Mo-rich M_6C carbides containing

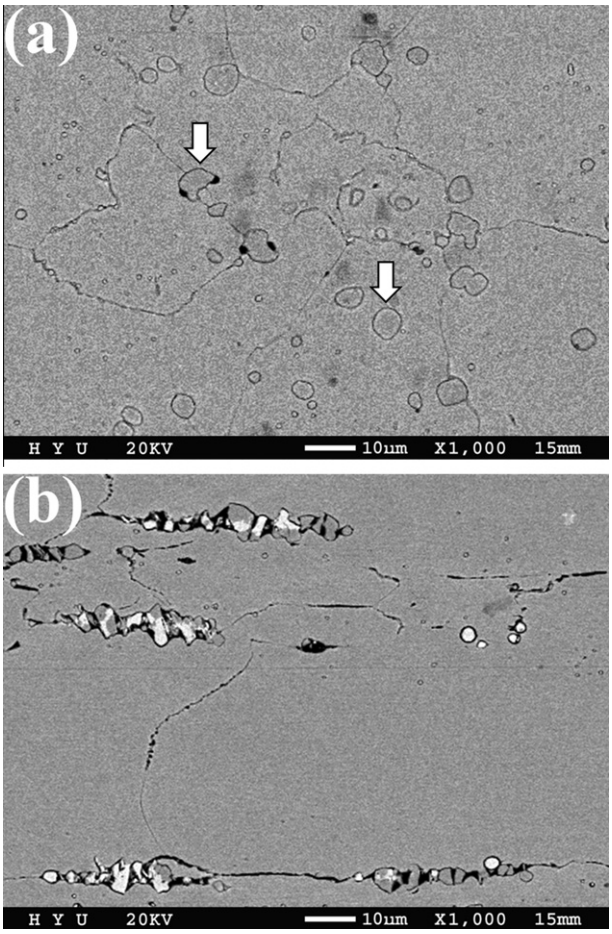

Fig. 2. BSE images of: (a) the as-received and (b) 50% cold-rolled Alloy 617.

13.9 at.% C, 23.4 at.% Cr, 7.1 at.% Co, 19.5 at.% Ni and 36.1 at.% Mo by EDS analysis.

The phases of Cr and Mo-rich carbides in the CR were confirmed via TEM analysis, as presented in Fig. 3. Two kinds of carbides were identified as Cr-rich (21.5 at.% C, 55.8 at.% Cr, 2.5 at.% Co, 9.5 at.% Ni and 10.7 at.% Mo) and Mo-rich carbides (14.5 at.% C, 16.8 at.% Cr, 9.8 at.% Co, 18.7 at.% Ni and 40.2 at.% Mo) according to the TEM equipped with EDS. The d-spacings of carbides was calculated using lattice fringe with selected area diffraction pattern (SADP). Fig. 3a shows the lattice fringe in the [1 1 0] zone axis of Cr-rich carbide and corresponding SADP. The d-spacing of the (0 0 2) plane was calculated as 0.5348 nm. Fig. 3b depicts the lattice fringe and SADP in the [2 1 0] zone axis of Mo-rich carbide, in which the d-spacing of the (0 0 2) plane was confirmed as 0.5607 nm. The lattice parameters of Cr and Mo-rich carbides were determined to be 1.070 nm ($M_{23}C_6$ carbide) and 1.121 nm (M_6C carbide) according to the d-spacing. The calculated lattice parameters of the carbides coincided with the values reported by several authors [9,10,17].

Fig. 4 indicates the area fraction of total carbides for the quantitative evaluation of carbide changes produced during 50% cold rolling. The relative area fractions of carbides in the AR and CR were changed by severe plastic deformation and were calculated using image analysis. The area fractions of total carbides ($M_{23}C_6$

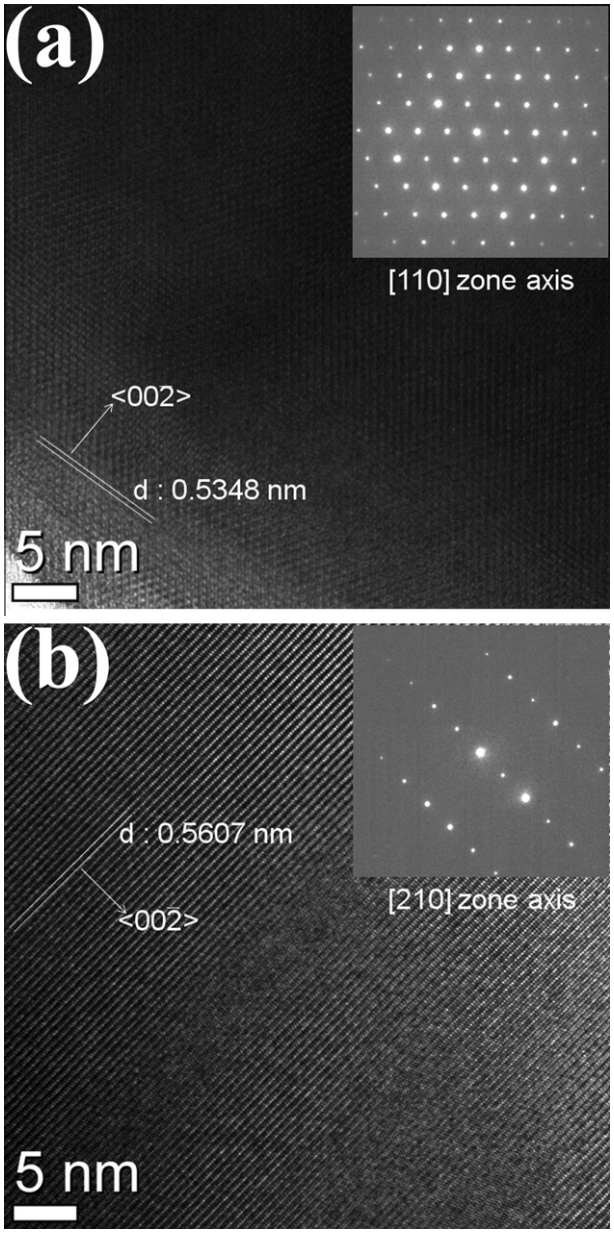

Fig. 3. TEM analyses of: (a) $M_{23}C_6$ carbide and (b) M_6C carbide in CR after 50% cold rolling.

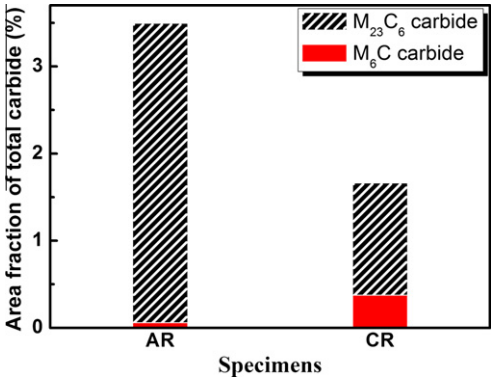

Fig. 4. Changes in the area fractions of $M_{23}C_6$ and M_6C carbides due to cold rolling.

and M_6C) in AR and CR were approximately 3.50% and 1.66%, respectively. The area fraction of $M_{23}C_6$ carbide in CR decreased from 3.44% (AR) to 1.29% (CR) during the severe plastic deformation. However, the area fraction of M_6C carbide increased from 0.06% (AR) to 0.37% (CR) even though the area fraction of $M_{23}C_6$ carbide decreased in CR. As a result, the area fraction of total carbides in CR predominantly decreased with decreasing area fraction of $M_{23}C_6$ carbide during 50% cold rolling. The area fraction change in carbides was associated with severe plastic deformation during cold rolling.

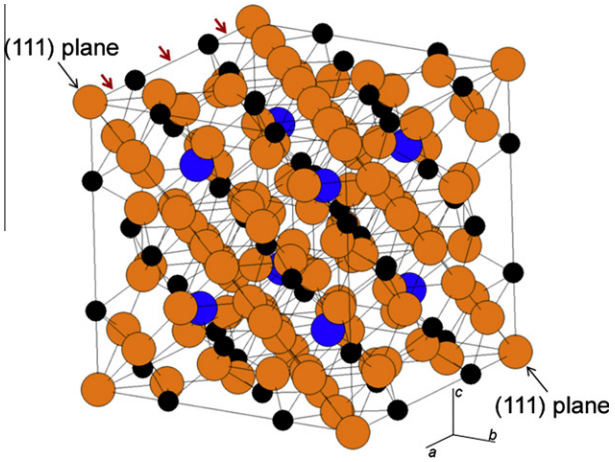

Fig. 5. The crystal structure of Cr-rich $M_{23}C_6$ carbide belongs to space group (Fm $\bar{3}$ m).

It has been reported that cementite in pearlitic steel is dissolved by severe plastic deformation during heavy cold working [13–16]. The driving force for the dissolution results from the higher interaction energy between dislocations generated during cold working and carbon atoms in cementite compared with the binding energy between carbon and iron atoms in cementite. The dislocations are preferentially stored at the ferrite–cementite interface during deformation. The carbon atoms in the cementite can be trapped by dislocations crossing the cementite lamellae or by dislocations located in ferrite near the ferrite–cementite interface during deformation. The $M_{23}C_6$ carbide in Alloy 617 may be dissociated similar to the dissolution of cementite in pearlitic steel by severe plastic deformation.

Fig. 5 shows the crystal structure of Cr-rich $M_{23}C_6$ carbide, which belongs to the space group (Fm $\bar{3}$m) [18]. The atoms in the unit cell of $M_{23}C_6$ carbide consist of 92 metals and 24 carbon atoms. The carbides crystallize in the cubic system with a face-centered lattice in which 92 metal atoms (orange and blue colors) are located at the 4*a*, 8*c*, and 32*f* and 48*h* symmetry sites of the Fm $\bar{3}$ m space group. As previously mentioned, the Cr-rich $M_{23}C_6$ carbide includes Mo atoms. The Mo atoms present in $M_{23}C_6$ carbide replace Cr at the 8*c* sites (blue[1] color) and result in more stable $M_{23}C_6$ carbide [19]. Additionally, the carbon atoms (dark color) are most reasonably placed at the 24*e* sites. $M_{23}C_6$ carbide had a perfect cube-on-cube orientation relationship with the fcc-Ni matrix [18].

The slip of the fcc-Ni matrix occurred in the ⟨1 1 0⟩ direction on the {1 1 1} plane due to shear stress generated during cold rolling. For fcc-$M_{23}C_6$ carbide, the slip also occurred on the {1 1 1} plane, as in the fcc-Ni matrix. As shown in Fig. 5, Cr atoms on the (1 1 1) plane in the $M_{23}C_6$ carbide had relatively weak bonding with Cr and C compared to the strengths of the Mo–Cr or Mo–C bonds [20]. During severe plastic deformation, a high density of dislocations was generated in the CR matrix and was confirmed by the higher internal microstrain, as calculated in Fig. 1. $M_{23}C_6$ carbides were fractured during the deformation, as shown in Fig. 2b. Thus, if

[1] For interpretation of color in Fig. 5, the reader is referred to the web version of this article.

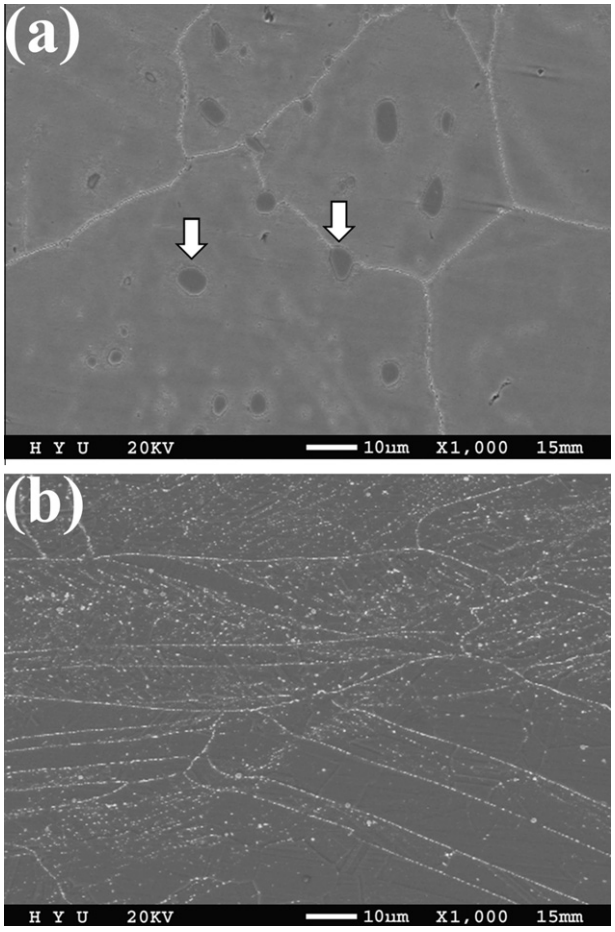

Fig. 6. SEM morphologies of: (a) AR and (b) CR after aging at 1050 °C without holding time.

the interaction energy between dislocations and C exceeds the binding energy of Cr–C on the (1 1 1) plane, the carbon atoms in Cr–C bond can be trapped by the dislocation crossing the $M_{23}C_6$ carbides during cold rolling. With the carbon trap, Cr atoms on the (1 1 1) plane can be dissolved in the matrix near the $M_{23}C_6$ carbide. Thus, severe plastic deformation made possible the dissociation of $M_{23}C_6$ carbides by the carbon traps around the dislocations.

The dissociation of $M_{23}C_6$ carbide in CR was also confirmed through further heat treatment. Fig. 6 shows the microstructure of heat-treated AR (HAR) and CR (HCR) after aging at 1050 °C at a heating rate of 10 °C/min without a holding time. There was not much change in the sizes or shapes of the carbides in HAR after heat treatment, as shown in Fig. 6a. In the case of HCR, fine carbides were newly precipitated at grain boundaries and inside the grain due to the heat treatment. The area fraction of total carbides in HCR was increased from 1.60% (CR) to 2.99% (HCR) because of re-precipitated fine carbides during the heat treatment. The phases of the fine carbides in the HCR were analyzed using TEM, as presented in Fig. 7 which shows the bright-field image of HCR after heat treatment. The size range of the fine carbides was confirmed as 100–500 nm. Fig. 7b depicts the high resolution TEM (HR-TEM) image in the [1 1 0] zone axis of the fine carbide. The d-spacing of the (0 0 2) plane in the [1 1 0] zone axis was calculated as 0.532 nm. Additionally, the chemical composition of fine carbide was confirmed as 19.7 at.% C, 54.8 at.% Cr, 3.2 at.% Co, 12.3 at.% Ni and 10 at.% Mo using TEM equipped with EDS. The fine carbides were confirmed to be Cr-rich $M_{23}C_6$ carbide through the analyses of d-spacing and chemical composition. The fine $M_{23}C_6$ carbides were re-precipitated in the HCR due to the reaction of Cr elements

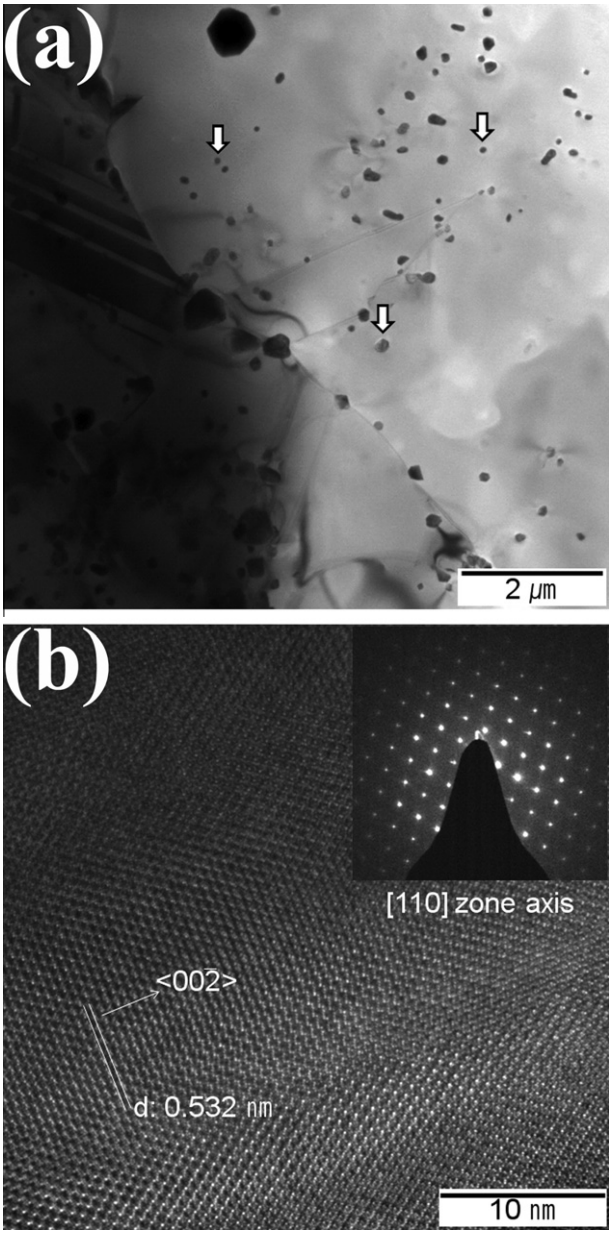

Fig. 7. The phase analyses on: (a) a bright-field TEM image and (b) an HR image in the [1 1 0] zone axis of the fine carbides in CR after aging at 1050 °C without a holding time.

dissolved in the matrix with carbons trapped by dislocations during the heat treatment.

The formation of M_6C carbide was induced by the dissociation of $M_{23}C_6$ carbide during severe plastic deformation. As shown in Fig. 4, the area fraction of $M_{23}C_6$ carbide in CR was decreased due to dissociation during severe plastic deformation, while the area fraction of M_6C carbide in CR increased. The increase of the area fraction of M_6C carbide was caused by relative changes in chemical compositions, such as Cr and Mo in the $M_{23}C_6$ carbides. It has been reported that the $M_{23}C_6$ carbide is transformed to M_6C carbide with increasing Mo content in $M_{23}C_6$ carbide [9–12]. The interaction of $M_{23}C_6$ and M_6C carbides occurs as follows:

$$M_{23}C_6 \underset{+Cr}{\overset{+Mo}{\rightleftharpoons}} M_6C. \quad (2)$$

The formation of $M_{23}C_6$ or M_6C carbide is controlled by the relative amounts of Cr and Mo in the carbide [9]. A similar reaction

occurred during the dissociation of $M_{23}C_6$ carbide by carbon traps in the dislocation. In the CR, the original Mo content in the $M_{23}C_6$ carbide relatively increased by decreasing the Cr content as Cr dissolved in the matrix during the dissociation of $M_{23}C_6$ carbide. The increased Mo content in $M_{23}C_6$ carbide induced the formation of M_6C carbide. Consequently, the carbon dissolution in the $M_{23}C_6$ carbide during severe plastic deformation induced the dissociation of $M_{23}C_6$ carbide and the formation of M_6C carbide in CR.

4. Conclusions

The cold-rolled Alloy 617 was oriented from the (1 1 1) plane to the (2 2 0) plane due to severe plastic deformation. Additionally, the high dislocation density that accumulated in the matrix was confirmed by the higher internal microstrain. The carbides in CR were distributed along the elongated grain boundary and were fractured during plastic deformation because of the stress applied during cold rolling. The carbides in AR and CR mainly consisted of $M_{23}C_6$ and M_6C. The area fraction of the total carbide in CR was greatly decreased because of the dissociation of $M_{23}C_6$ carbides during severe plastic deformation, and the area fraction of M_6C carbide in CR increased during the dissociation of $M_{23}C_6$ carbide. The severe plastic deformation induced the dissociation of $M_{23}C_6$ carbides and the formation of M_6C carbide.

Acknowledgment

This work was financially supported by the Ministry of Education, Science and Technology (MEST) of the Republic of Korea, through the Nuclear Hydrogen Technology Development (NHTD) Program.

References

[1] P.S. Shankar, K. Natesan, J. Nucl. Mater. 366 (2007) 28–36.
[2] P. Yvon, F. Carre, J. Nucl. Mater. 385 (2009) 217–222.
[3] S. Chomette, J.-M. Gentzbittel, B. Viguier, J. Nucl. Mater. 399 (2010) 266–274.
[4] T.H. Bassford, J.C. Hosier, Nucl. Technol. 66 (1984) 35–43.
[5] T. Hirano, M. Okada, H. Araki, T. Noda, H. Yoshida, R. Watanabe, Metall. Trans. A 12 (1981) 451–458.
[6] S. Kihara, J.B. Newkirk, A. Ohtomo, Y. Saiga, Metall. Trans. A 11A (1980) 1019–1031.
[7] W. Ren, R. Swimdeman, A review of aging effects in alloy 617 for Gen IV nuclear reactor applications, ASME pressure vessels and piping division conference, in: Proceedings of PVP 2006-ICPVT-11-93128, 2006.
[8] T. Takahashi, J. Fujiwara, T. Matsushima, M. Kiyokawa, I. Morimoto, T. Watanabe, Trans. ISIJ 18 (1978) 221–224.
[9] C.T. Sims, N.S. Stoloff, W.C. Hagel, Superalloys II, John Willey & Sons, New York, 1987. pp. 111–117.
[10] H.J. Goldschmidt, Interstitial Alloy, Plenum, New York, 1967. pp. 101–114.
[11] A.F. Padilha, P.R. Rios, ISIJ Int. 42 (2002) 325–337.
[12] B. Weiss, R. Stickler, Metall. Trans. 3 (1972) 851–866.
[13] V.N. Gridnev, V.V. Nemoshkalenko, Yu. Ya. Meshkov, V.G. Gavrilyuk, V.G. Prokopenko, O.N. Razumov, Phys. Status Solidi (A) 31 (1975) 201–210.
[14] V.N. Gridnev, V.G. Gavrilyuk, Phys. Metals (1983) 531–551.
[15] V.G. Gavriljuk, Mater. Sci. Eng. A 345 (2003) 81–89.
[16] V.G. Gavriljuk, Scripta Mater. 24 (2002) 175–177.
[17] B.D. Cullity, S.R. Stock, Elements of X-ray Diffraction, third ed., Prentice-Hall, New Jersey, 2001. pp. 174–177.
[18] J.-C. Zhao, M. Larsen, V. Ravikumar, Mater. Sci. Eng. A 293 (2000) 112–119.
[19] S.G. Hong, W.B. Lee, C.G. Park, J. Nucl. Mater. 288 (2001) 202–207.
[20] J. Xie, J. Shen, N. Chen, S. Seetharaman, Acta Mater. 54 (2006) 4653–4658.